Tetrahedron 64 (2008) 7407–7418

Contents lists available at ScienceDirect

Tetrahedron

journal homepage: www.elsevier.com/locate/tet

A computational study and valence bond approach to the intramolecular electrophilic aromatic substitution mechanism of *ortho*-allyl-*N*-benzylanilines

Elena E. Stashenko [a], Jairo R. Martínez [a], Geovanna Tafurt-García [a], Alirio Palma [b], Josep Maria Bofill [c,*]

[a] *Laboratorio de Cromatografía, Centro de Investigación en Biomoléculas, CIBIMOL, Escuela de Química, Universidad Industrial de Santander, Cra 27 Calle 9, Bucaramanga, Colombia*
[b] *Laboratorio de Síntesis Orgánica, Centro de Investigación en Biomoléculas, CIBIMOL, Escuela de Química, Universidad Industrial de Santander, Cra 27 Calle 9, Bucaramanga, Colombia*
[c] *Departament de Química Orgànica i, Institut de Química Teòrica i Computacional (IQTCUB), Universitat de Barcelona, Martí i Franquès 1, 08028 Barcelona, Catalunya, Spain*

ARTICLE INFO

Article history:
Received 3 March 2008
Received in revised form 7 May 2008
Accepted 8 May 2008
Available online 13 May 2008

ABSTRACT

Ab initio computational studies were performed for the intramolecular Friedel–Crafts alkylation of *ortho*-allyl-*N*-benzylanilines catalyzed by sulfuric acid, which results in the formation of both dihydrodibenz[*b*,*e*]azepine and tetrahydrodibenz[*b*,*f*]azocine isomers. This intramolecular reaction occurs through the rearrangement of the cationic species generated from the allyl moiety and falls into the type of electrophilic aromatic substitution rearrangements. Due to this fact, we discuss the reactivity trends of the intermediate species participated in this competitive 7-*exo*-*trig* versus 8-*exo*-*trig* cyclization process. The valence bond configuration mixing is used for this purpose and with this model the reduced potential energy surface and the reaction profile are constructed. The expected patterns such as single step or stepwise mechanism, and the trends in the reaction barriers for the electrophilic attack effects of the aryl substituents are discussed.

1. Introduction

The dibenz[*b*,*e*]azepine ring and its derivatives have attracted interest within the organic chemistry community due to their importance as bioactive agents for the treatment of depression, anxiety, allergies, and other disorders.[1–8] Anthranilic acid and *ortho*-aminobenzylic alcohol derivatives, among others, have been proposed as precursors for the construction of the dibenz[*b*,*e*]azepine ring.[4,9,10] Recently, Kouznetsov et al.[11,12] described an alternative synthetic procedure based on the combination of the amino-Claisen rearrangement of *N*-allyl-*N*-benzylanilines and the intramolecular Friedel–Crafts alkylation of *ortho*-allyl-*N*-benzylanilines. The Friedel–Crafts step is catalyzed by concentrated sulfuric acid for about 2 h and heated at 90 °C. In these strong acidic conditions a stable benzyl cation is generated, which reacts immediately with the benzene ring and the intramolecular alkyl-cyclization product is obtained. The resulting product finally is extracted and purified by means of silica gel column chromatography procedure. Further studies on the intramolecular Friedel–Craft alkylation promoted by concentrated sulfuric acid revealed that important quantities of tetrahydrodibenz[*b*,*f*]azocine are formed together with the desired dihydrodibenz[*b*,*e*]azepine. Normally, the tetrahydrodibenz[*b*,*f*]-azocine derivatives are prepared by using methods that differ from the Friedel–Crafts alkylation.[13,14] Scheme 1 shows a proposed mechanism for the intramolecular Friedel–Crafts alkylation of the title compounds with sulfuric acid, which also explains the formation of dihydrodibenz[*b*,*e*]azepine and tetrahydrodibenz[*b*,*f*]azocine rings.

The formation of tetrahydrodibenz[*b*,*f*]azocine **5** is possible via an 8-*exo*-*trig* intramolecular cyclization of secondary carbocation **3**. The benzylic carbocation **6** is generated by a 1,2 hydride migration (1,2-H) of **3** and it is responsible for the formation of dihydrodibenz[*b*,*e*]azepine **8** by means of a 7-*exo*-*trig* intramolecular cyclization. The product distribution for this reaction is explained based on the interplay of the thermodynamic and kinetic control. In general, it is assumed that the formation of dihydrodibenz[*b*,*e*]-azepine is a result of thermodynamic control, whereas the formation of tetrahydrodibenz[*b*,*f*]azocine is determined by kinetic control.[12] However, the kinetic measurements of this reaction are not sufficient to obtain a mechanistic model, which can explain the formation of both constitutional isomers. Due to this fact, here, it is reported a theoretical quantum mechanical study of the potential energy surface associated with this reaction.

The quantum mechanical calculations normally do not provide new conceptual insight about the central set of questions on the reactivity. In other words, they do not give in a clear way the factors

* Corresponding author.
E-mail address: jmbofill@ub.edu (J.M. Bofill).

0040-4020/$ – see front matter © 2008 Elsevier Ltd. All rights reserved.
doi:10.1016/j.tet.2008.05.023

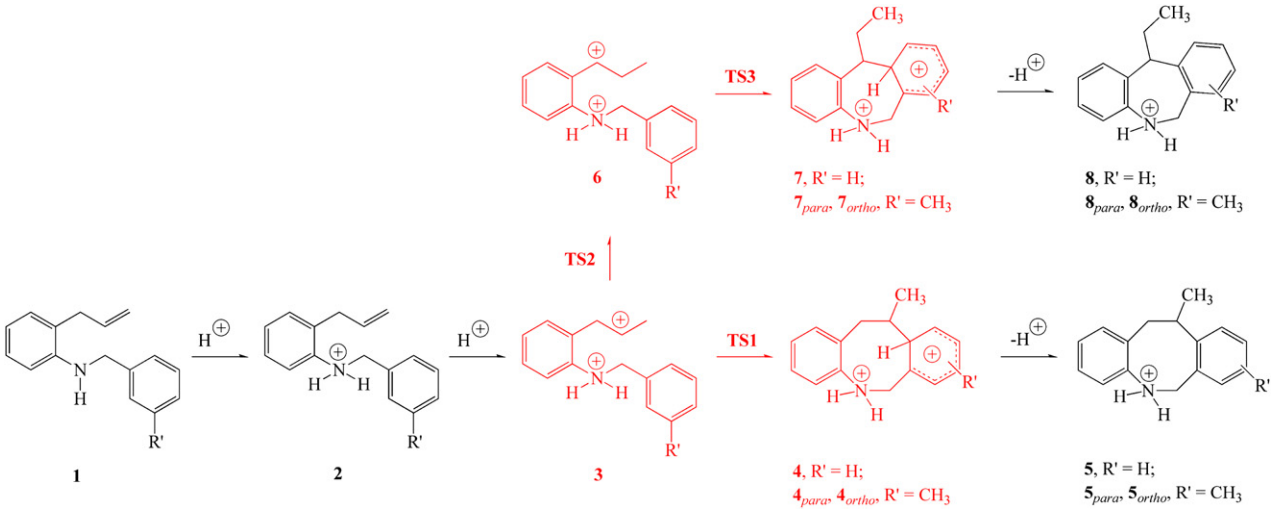

Scheme 1.

or causes that govern the form and the shape of a reaction profile, e.g., how large will an energy barrier be, or what is the nature and structure of the transition states (TSs), or will intermediates appear and if they appear what about their structures and finally, what is the effect of the substituents and solvents on the TSs and possible intermediates. An important step in this direction was the introduction of the reduced potential energy surface model (RPES) made by Thornton[15] and others.[16–22] This model attempts to give a qualitative estimation of the effects of the substituents and solvents on the modification of the TSs' geometries and their energy barriers of each mechanistic step. Basically, in this model a flexible PES is defined and characterized by reactants, products, and two intermediate stationary points. If the reactants are modified due to the changes on the substituent or solvent then the effects are transmitted through the PES resulting in changes in the position of the TSs. The modifications of the positions of the TSs in the PES or what is the same their geometries are consequence of the assumed flexibility of the PES. The degree of flexibility is a function of the changes on the substituent or in the solvent. The RPES model formulated in an appropriate mathematical form has been used also for computational aims, e.g., to locate reaction paths and TSs.[23,24] However, it is possible to show that a selected RPES perhaps does not connect in a continuous way with the regions of the full potential energy surface,[25] which are crucial in the description of the reaction process. The latter can be seen as a possible drawback of the RPES model. According to the RPES model the Friedel–Crafts reaction is characterized by two bond distances, namely, the bond distance between the electrophilic center to the aryl group, denoted by E and Ar, respectively, and the bond distance that characterizes the acid–base step, B···H···Ar, B being the basis. At first glance, the RPES model indicates that the Friedel–Crafts reaction can evolve across three different mechanisms, a concerted or single step and two stepwise routes. This fact implies that the surface of the RPES model has four minima and five TSs. The minima are the reactants, products, Wheland complex, which is a benzenium or cyclohexadienylium type carbocation, and the σ-aryl carbanion. All the minima are interconnected through a path except the two intermediates. Each path has the corresponding TS. In Figure 1 is shown the More O'Ferrall–Albery–Jencks diagram that can be used to explain the RPES of intramolecular Friedel–Crafts alkylations or electrophilic aromatic substitutions. Throughout the article by R′ will be denoted an aryl substituent. The More O'Ferrall–Albery–Jencks diagrams are widely used to represent the RPES model.[16–19]

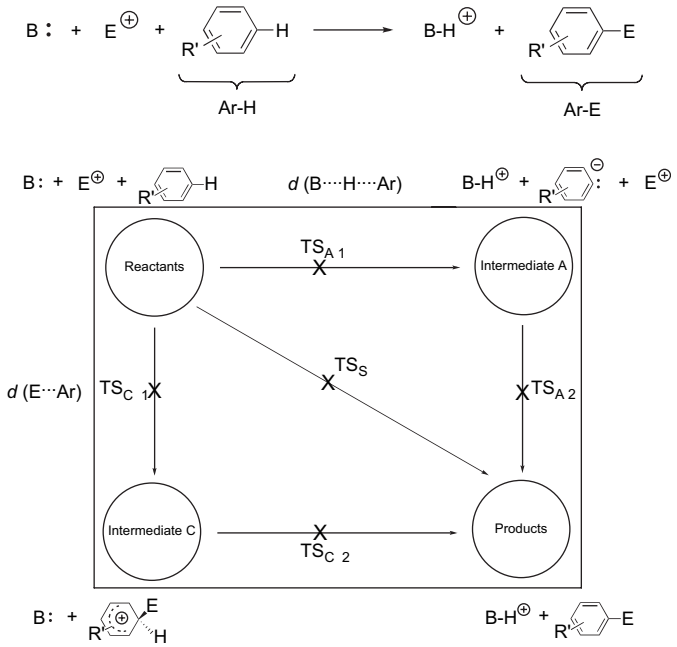

Figure 1. The More O'Ferrall–Albery–Jencks diagram of the reduced potential energy surface (RPES) of an electrophilic aromatic substitution reaction as a function of lengths of the bonds (B···H···Ar) and (E···Ar). The reaction only occurs through the intermediate C pathway, however, the other two possible pathways are also indicated. The intermediate C involves a benzenium cation or Wheland complex. The intermediate A is characterized among others by a σ-type aryl carbanion, which is completely non-estable being that the reason why this pathway is not favored. The TS_S is the transition state of the synchronous path, the bond breaking, B···H···Ar, and the bond formation, E···Ar, occur simultaneously.

Other model proposed to answer the above-mentioned central set of questions on reactivity is the Valence Bond Configuration Mixing (VBCM) of Pross and Shaik,[22,26] which is close in its form to the just outlined RPES model. In VBCM model the potential energy reaction profile is build by a blend of many-potential energy curves. Two of these potential energy curves are related with the valence bond configurations of reactants and products but also additional configurations are taken into account. These extra or additional configurations are not important in the energy and structure description of reactants and products, but can mix with these

configurations in the avoided crossing points, which are located in the TS region. Since an avoided crossing point is near to the TS, then the resulting configuration mixing at this point gives information about the energy and structure of the TS.[22,27,28] In a few words, for the VBCM model a TS structure is a hybrid of many valence bond structures where two of them are the valence bond of reactants and products. The VBCM model or modifications from it has been used several times in different chemical problems.[29–36] Specifically, Shaik et al. have reported important applications of this theory in different chemical situations.[28]

In this article, it is studied from a quantum computational point of view the mechanism of steps in shaded red areas in Scheme 1, taking into account all the previous comments in a way to analyze it. The results are extended to a general reaction of electrophilic aromatic substitution. The factors that govern the proposed mechanism and the chemical insight will be analyzed using the RPES and VBCM models. In order to overlap the two models, we associate to each minimum of the RPES surface, namely, reactants, products, Wheland complex and σ-aryl carbanion, a valence bond configuration, VB, denoted by Φ_R, Φ_P, Φ_{IC}, Φ_{IA}, respectively (Scheme 2). For reasons discussed in the next section, the VB notation for reactants and products configuration, Φ_R and $\Phi_{HL}(R)$, Φ_P and $\Phi_{HL}(P)$, will be used indifferently.

The VB configurations are depicted as a function of the groups, E, Ar, H, B (Scheme 2). The relation of these groups with the molecule or part of the molecule of the present study is given in Scheme 3.

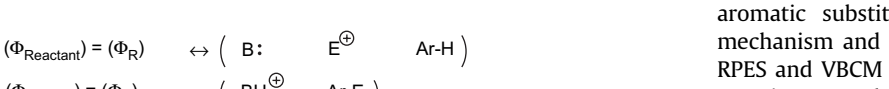

E = electrophilic group;
Ar = aryl group used indiferently with or without substituents which are denoted by R';
H = hydrogen that in the products forms BH;
B = bases

Scheme 2.

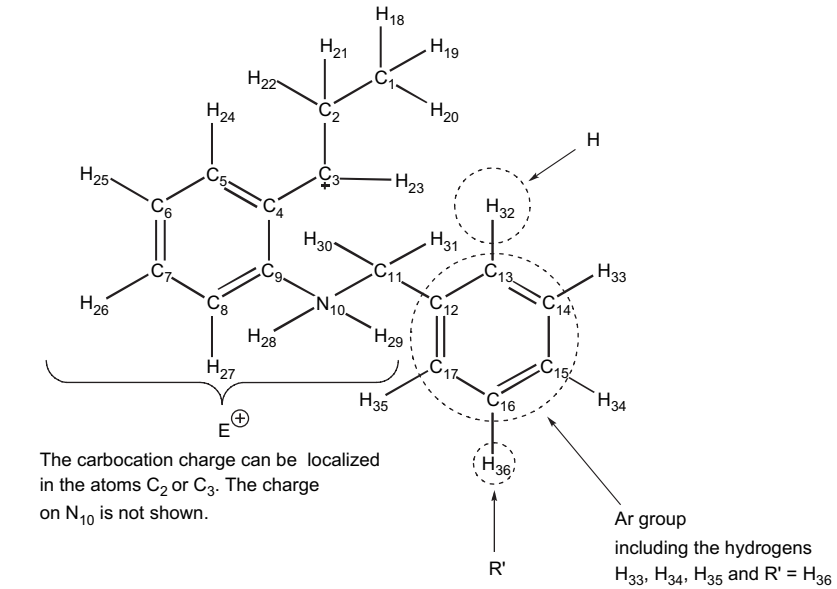

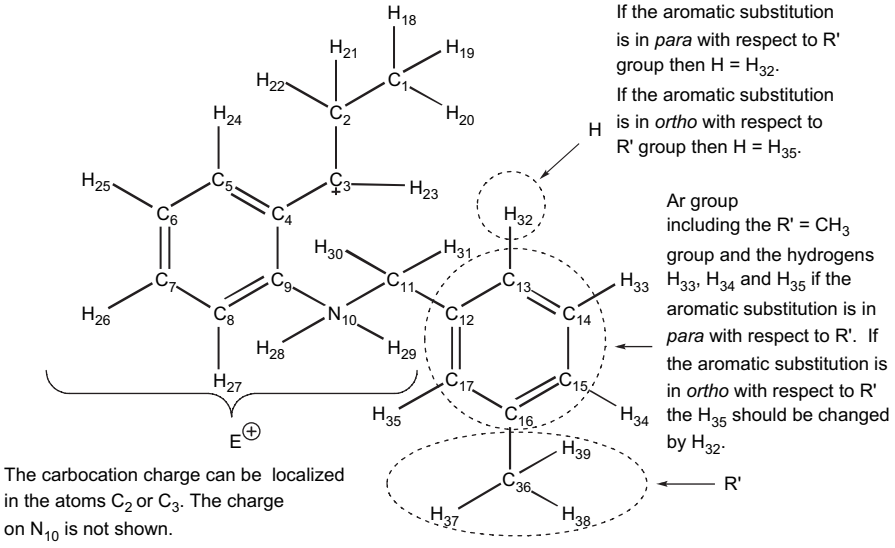

Scheme 3.

2. Computational procedure and methodology

The computational tasks were performed with the Gaussian 03[37] suite of programs. The 6-31+G(d) basis set was used to optimize all the molecular structures[38] and 6-311++G(d,p) for energies.[38c,39] These basis sets are deemed suitable for the molecular system under consideration.

The molecular geometries of reactants, products, intermediates, and transition states depicted in Scheme 1 were optimized by gradient methods and tested by frequency calculations using analytical second derivatives. All molecular structure optimizations were carried out at the unrestricted Hartree–Fock (UHF) SCF level of theory. Energies were determined at RMP2 (full)/6-311++G(d,p) level, the latter including also the core electrons to the energy correlation correction.

The wave function associated to the avoided crossing points was evaluated according to the method reported by Shaik and Reddy.[27] First, the group charges were assigned on the basis of natural bond orbitals (NBOs)[40,41] at the UHF level. Second, using these charges the coefficients of the VBCM contributions of the wave function are evaluated. Finally, the resulting wave function served to describe the electronic structure of the TS in terms of the avoided crossing points. Notice that in this way we obtain a wave function satisfying the avoided crossing restrictions and constructed from VB configurations. The resulting VBCM wave function is closest to the desired TS wave function (Ψ_{TS}), then it can be expressed approximately by the wave function of the state (Ψ_{ACS}) associated to an avoided crossing point. In terms of wave function the latter can be written as[22,27]

$$\Psi_{TS} \approx \Psi_{ACS} = \left(1+\sum_{I=1}^{N} c_I^2\right)^{-1/2} \left\{2^{-1/2}[\Phi_{HL}(R)+\Phi_{HL}(P)]+\sum_{I=1}^{N} c_I\Phi_I\right\} \quad (1)$$

In Eq. 1, $\Phi_{HL}(R)$ and $\Phi_{HL}(P)$ are the Heitler–London VB configurations that describe the covalent bonding structures of reactants and products, respectively. The set $\{\Phi_I\}_{I=1}^{N}$ is formed by the VB configurations each one describing intermediate structures (ionic or covalent) and contributing to the description of the avoided crossing state. We emphasize the notation that $\Phi_{HL}(R)$ and $\Phi_{HL}(P)$ are equal to Φ_R and Φ_P, respectively. The contribution of the intermediate VB configurations is quantified by the set of coefficients $\{c_I\}_{I=1}^{N}$. Notice that in the VB configurations of reactants, $\Phi_{HL}(R)$, and products, $\Phi_{HL}(P)$, contribute equally to the Ψ_{ACS} of Eq. 1. As Shaik and coworkers pointed out,[27] in the region of the PES where the reaction takes place, there exist a point on this PES where the wave function represented by the set of VB configurations, $\Phi_{HL}(R)$, $\Phi_{HL}(P)$ and $\{\Phi_I\}_{I=1}^{N}$, has the form given in Eq. 1 and this point is labeled avoided crossing point. The avoided crossing point is then a point on the potential energy reaction profile that lies directly beneath the crossing point described exclusively by the VB structures $\Phi_{HL}(R)$ and $\Phi_{HL}(P)$. Due to the proximity between avoided crossing point and TS, in the potential energy surface, the wave function in the avoided crossing point, Ψ_{ACS}, must look alike as the wave function in the TS, Ψ_{TS}, which takes the following form in the same VB representation

$$\Psi_{TS} = c'_R\Phi_{HL}(R)+c'_P\Phi_{HL}(P)+\sum_{I=1}^{N} c'_I\Phi_I \quad (2)$$

Following Shaik et al.,[22,27] to summarize and clarify the above ideas we say that the avoided crossing point can be seen such a transition point between reactants and products wave functions (electronic distributions) that characterize an elementary mechanistic step. The nature of both, the geometry associated to the avoided crossing point located in the PES and their wave function given in Eq. 1 makes this concept an ideal form to analyze the TS paradigm from the structure and electronic distribution point of view, provided that the TS point and the avoided crossing point are neighborhood points in the PES. We define an elementary mechanistic step as the set of changes of an evolutionary molecular system that using the reaction path model[22,42] they can be described by a path on the PES associating each configuration to a point of this path. This path located on the PES starts in a stationary point character minimum and connects in a continuous way with other stationary point character minimum through a stationary point with character first order saddle point. In addition, no other type of stationary point of any character can be found through this path connecting these two minima.

Finally, we emphasize that the proximity between the TS and the avoided crossing point in the region of the PES related with the mechanism under consideration are underlying in the above procedure and the model. In the avoided crossing point the wave function has the structure Ψ_{ACS} given in Eq. 1. The electronic state of the avoided crossing point described by the Ψ_{ACS} wave function is endowed with a delocalization energy gained due to the VB configuration mixing that generates this electronic state. The above Ψ_{ACS} wave function was formulated for the description of the avoided crossing points associated to elementary mechanistic steps. Following the vision of localized picture, we want to generate a more general Ψ_{ACS} wave function from the VB configuration mixing for the description of avoided crossing points corresponding to a reaction process that involves a sequence of elementary mechanistic steps. From this point of view, a stepwise reaction occurs when the structures described by the set of Φ_I configurations are more stable than the crossing points formed by Heitler–London VB configurations. This fact implies the existence of crossing points formed by a Heitler–London VB configuration and a Φ_I configuration. In this manner the intermediate structures provide a reaction path of lower potential energy than mediating the whole reaction process. This reaction path is characterized by the transformation of the fundamental VB configuration, that it is from $\Phi_{HL}(R)$ to $\Phi_{HL}(P)$. The localized wave functions that at the limits of the reaction process become simple Heitler–London configurations, $\Phi_{HL}(R)$ and $\Phi_{HL}(P)$, are given by the equations

$$\Psi_R = \left(1+2^{-1}\sum_{I=1}^{N} r_I^2\right)^{-1/2}\left\{\Phi_{HL}(R)+2^{-1/2}\sum_{I=1}^{N} r_I\Phi_I\right\} \quad (3)$$

$$\Psi_P = \left(1+2^{-1}\sum_{I=1}^{N} p_I^2\right)^{-1/2}\left\{\Phi_{HL}(P)+2^{-1/2}\sum_{I=1}^{N} p_I\Phi_I\right\} \quad (4)$$

The bonding and antibonding combinations of Ψ_R and Ψ_P wave functions yield the Ψ and Ψ^*, respectively,

$$\Psi = w_R\Psi_R + w_P\Psi_P \quad (5)$$

$$\Psi^* = w^*_R\Psi_R - w^*_P\Psi_P \quad (6)$$

Thus, the Ψ wave function describes an electronic state such that normally the structures associated to the Φ_I VB configurations are higher in energy with respect to the Heitler–London structures in the regions of the PES associated to reactants and products. However, along the reaction path region the energy curves associated to the Heitler–London structures interchange, while the energy curves associated to the Φ_I VB configurations correlate horizontally

and cross the energy curves of the two Heitler–London structures either above or below their crossing point.[27,28] In the avoided crossing points, the bonding wave function takes the form of $\Psi=\Psi_{ACS}\approx\Psi_{TS}$, whereas the antibonding one is $\Psi_*=\Psi_{\bar{A}CS}=2^{-1/2}[\Phi_I-\Phi_J]$, being Φ_I and Φ_J the VB configurations that mix strongly and they define the Heitler–London resonating state in this region of the PES. This scheme will be depicted and explained in Section 4 for the present type of reaction.

3. Computational results

3.1. Relative energies and potential energy reaction profiles

We start the study of the mechanism of transformation of the dication compound **3** (compound numbering according to Scheme 1). Figure 2A and B shows the potential wells for the reaction that transforms **3** to tetrahydrodibenz[*b*,*f*]azocine, **5**, and **3** to dihydrodibenz[*b*,*e*]azepine, **8**, for R′=H and R′=CH_3. For both reactions the last steps, namely, from **4** to **5** and from **7** to **8**, were not computed since they are merely acid–base rearrangements.

In Tables 1 and 2 we report the relative energies of the critical points corresponding to the potential energy reaction profiles shown in Figure 2A and B. Regarding the potential wells for R′=H, either, the benzylic carbocation **6**, also known as Wheland complex,[43,44] is more stable than the intermediate carbocation **3**. This energetic stabilization reflects the established fact that a molecular structure with delocalized charge is more stable than the corresponding isomer structure with localized charge.[43,44] However, the Wheland type complex intermediates, **4** and **7**, are less stable than their precursors, the carbocation **3** and benzylic carbocation **6**, respectively.

The shape of the reaction profiles is different for R′=CH_3. In this case, **6** and the Wheland complexes, $\mathbf{4}_{ortho}$ and $\mathbf{4}_{para}$, are more stable than **3**, while, the Wheland complex $\mathbf{7}_{para}$ is more stable than its precursor **6**, and $\mathbf{7}_{ortho}$ is less stable than it. In addition to that, $\mathbf{7}_{para}$ is more stable than $\mathbf{4}_{ortho}$ and $\mathbf{4}_{para}$, while $\mathbf{7}_{ortho}$ is the less stable Wheland complex of all. The subscripts $\mathbf{4}_{ortho}$, $\mathbf{4}_{para}$, mean that for R′=CH_3, the methyl radical is localized in position *ortho* or *para* with respect to the tetravalent carbon, respectively.

The transformation of carbocation **3** to the benzylic cation **6** is merely a 1,2 hydride shift. Despite that the benzylic cation **6** is much more stable than species **3**, the energy barrier for the formation of the benzylic cation **6** from the carbocation **3** is much higher in energy than the barrier of the formation of the Wheland complexes, **4**, from the carbocation, **3** (with the exception of R′=H, where the barrier energy of the transformation is similar), but lower with respect to the formation of the Wheland complexes **7** from benzylic cation **6**.

From inspection of Tables 1 and 2 we conclude first that the methyl radical favors the formation of **5** and **8** with respect to the reaction with unsubstituted aromatic ring. Second, from a kinetic point of view the formation of **5**, both *ortho* and *para* approximations, is favored with respect to the formation of **8**. In either case, the step of formation of Wheland complex intermediate **4** is that involves lower activation energy as noted before.

From an inspection of Figure 2 we formulate the following general question, what is the relationship between a molecule with many conjugated constitutional isomers, such as carbocation rearrangements and its properties? This question can be formulated in a more concise way: how much will the magnitude of rate constant between carbocations, k_{36} and k_{63}, affect a molecular property? The situation then examines the relationship between a molecule's carbocations related by transposition and its chemical reactivity is illustrated in Scheme 4, which is basically a Curtin–

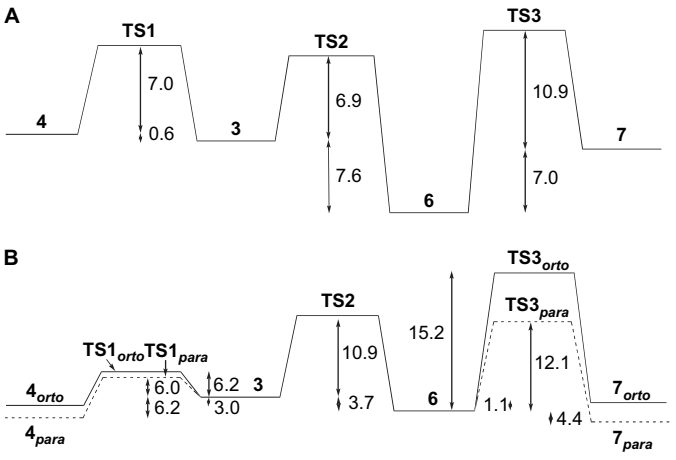

Figure 2. (A) Potential energy reaction profile for the formation of Wheland intermediates for R′=H. The structures are numbering according to Scheme 1. The potential energy values are given in kcal/mol and correspond to that given in Table 1. (B) Potential energy reaction profile for the formation of Wheland intermediates for R′=CH_3. The structures are numbering according to Scheme 1. The potential energy values are given in kcal/mol and correspond to that given in Table 2.

Table 1
The calculated relative energies of the stationary points, reaction energies, and energy barriers for the set of elementary reactions with R′=H[a]

Reaction[b]	Reactant	TS[c]	Product	E_r[d] (Reac.→Prod.)	E_a[e] (Reac.→Prod.)
3→**6**	7.6	14.5 (**TS2**)	0.0	−7.6	6.9
3→**4**	7.6	15.2 (**TS1**)	8.2	0.6	7.6
4→**5**	8.2		124.4	116.2	
6→**7**	0.0	17.9 (**TS3**)	7.0	7.0	17.9
7→**8**	7.0		116.9	109.9	

[a] In kcal/mol.
[b] Structure numbering according to Scheme 1.
[c] Within parenthesis the numbering of the transition state structure according to Scheme 1.
[d] Reaction energy.
[e] Energy barrier.

Table 2
The calculated relative energies of the stationary points, reaction energies, and energy barriers for the set of elementary reactions with R′=CH_3[a]

Reaction[b]	Reactant	TS[c]	Product	E_r[d] (Reac.→Prod.)	E_a[e] (Reac.→Prod.)
3→**6**	8.1	19.0 (**TS2**)	4.4	−3.7	10.9
3→$\mathbf{4}_{ortho}$	8.1	14.3 ($\mathbf{TS1}_o$)	5.1	−3.0	6.2
3→$\mathbf{4}_{para}$	7.6	13.6 ($\mathbf{TS1}_p$)	1.4	−6.2	6.0
$\mathbf{4}_{ortho}$→$\mathbf{5}_{ortho}$	5.1		140.3	135.2	
$\mathbf{4}_{para}$→$\mathbf{5}_{para}$	1.4		127.7	126.3	
6→$\mathbf{7}_{ortho}$	4.4	19.6 ($\mathbf{TS3}_o$)	5.5	1.1	15.2
6→$\mathbf{7}_{para}$	4.4	16.5 ($\mathbf{TS3}_p$)	0.0	−4.4	12.1
$\mathbf{7}_{ortho}$→$\mathbf{8}_{ortho}$	5.5		124.3	118.8	
$\mathbf{7}_{para}$→$\mathbf{8}_{para}$	0.0		120.2	120.2	

[a] In kcal/mol.
[b] Structure numbering according to Scheme 1.
[c] Within parenthesis the numbering of the transition state structure according to Scheme 1. The subscripts *o* and *p* mean *ortho* and *para*, respectively.
[d] Reaction energy.
[e] Energy barrier.

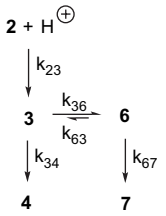

Scheme 4.

Hammett (C–H)/Winstein–Holness (W–H) kinetic system.[45] The so-called Curtin–Hammett/Winstein–Holness enunciate and the associated kinetic schemes were established for the first time to relate molecule conformations with its chemical reactivity.[45a,45c] However, it has been shown that it can be applied to different chemical situations,[45e] the latter represents a new example.

If the conversion between **3** and **6** is extremely rapid with respect to the transformation from **3** to **4** and from **6** to **7**, then one says that the system behaves as described in the Curtin–Hammett/Winstein–Holness enunciate. In the opposite extreme situation, if the conversion between **3** and **6** is substantially lower than the transformation from **3** to **4** and from **6** to **7**, one says that the system shows an anti-Curtin–Hammett/Winstein–Holness behavior. Between these two extreme cases exists an intermediate situation. These three cases were studied for the first time by Zefirof.[45d,45e] If we apply the above considerations to the present system, which possesses carbocations related by transpositions, we observe from Figure 2A that for R′=H, the process for the formation of Wheland intermediates **4** and **7** satisfies the intermediate situation between a Curtin–Hammett/Winstein–Holness and an anti-Curtin–Hammett/Winstein–Holness behavior corresponding to a kinetic scheme like that described in Scheme 4. Once **3** is formed its transformation to **6** and **4** is kinetically equal favored, and the same occurs when **6** is formed, its transformation to **3** and **7** is also kinetically equal favored. However, for R′=CH_3 the reaction occurs through an anti-Curtin–Hammett/Winstein–Holness[45d] kinetic scheme where the species **3** and **6** are not equilibrated favoring the formation of Wheland intermediates $\mathbf{4}_{ortho}$ and $\mathbf{4}_{para}$ in front of the benzylic carbocation **6** and consequently the two Wheland complexes, $\mathbf{7}_{ortho}$ and $\mathbf{7}_{para}$. Figure 2B represents a potential energy profile, such that its kinetics behaves as an anti-Curtin–Hammett/Winstein–Holness scheme.[45d]

3.2. Optimized molecular geometries

Table 3 lists the set of principal geometry parameters of the stationary points of the PES associated to the reaction under study for R′=H and R′=CH_3. Now, we focus the interest on the structure of the TSs and the intermediates.

The case with R′=H is the easiest model for a Friedel–Crafts intramolecular alkylation. The bond distance C_2–H_{22} in the transition state **TS2** related with the 1,2-hydrogen migration process is 1.325 Å, for R′=H while for R′=CH_3 is 1.332 Å, atom numbering is that given in Scheme 3. As expected the changes in R′ do not affect the main structure of the transition state for this 1,2-hydrogen shift reaction.

In the transition state for the Wheland complex intermediate formation the $C^{\oplus}$–C_{Ar} bond length, being C_{Ar} a carbon atom of the aromatic ring that at the products is linked with E, may be varies depending on two factors, the carbocation's nature and the substituted effects on the aromatic ring. In the present study C_{Ar} represents either the C_{13} or the C_{17} aromatic carbon atom according to the notation given in Scheme 3. For the case with R′=H, with the positive charge localized on the carbocation, the bond distance, C_2–C_{13}, at the **TS1** is 2.181 Å, while for the carbocation with delocalized positive charge, the bond distance, C_3–C_{13}, at the **TS3** is 2.195 Å. The bond breaking/bond formation, $C^{\oplus}$–C_{Ar}, is slightly larger when the carbocation is stabilized with respect to the non-stabilized analogous. For the case of R′=CH_3, there exist four situations generated by the *ortho* and *para* approaches. When the substitution occurs in *ortho* position, which is in the carbocation that has the localized positive charge, the critical bond distance, C_2–C_{17}, at the transition state, $\mathbf{TS1}_{ortho}$, is 2.322 Å, while for delocalized positive charge situation the critical bond distance, C_3–C_{17}, at the transition state, $\mathbf{TS3}_{ortho}$, is in the same range of the previous case, namely, 2.277 Å. On the other hand, for the substitution in *para* position, the crucial bond distance, C_2–C_{13}, at the $\mathbf{TS1}_{para}$, is 2.342 Å, for the case of localized positive charge, whereas for delocalized positive charge, the bond distance, C_3–C_{13}, at the $\mathbf{TS3}_{para}$, is 2.324 Å. We conclude that for the formation of the Wheland complex, the $C^{\oplus}$–C_{Ar} bond at the transition state does not change in a significant manner if the carbocation possesses or not a localized positive charge. The main effect in the $C^{\oplus}$–C_{Ar} bond distance at the transition state is due to the substituents in the aromatic ring. If an H atom is changed by a CH_3 radical, the $C^{\oplus}$–C_{Ar} bond enlarges by about 0.1 Å.

3.3. The electron density evolution: transition state and intermediate charges

The UHF NBO charges of the groups, E, Ar, and H, as defined in Scheme 3, for transition states and intermediates are reported in Tables 4–6. The NBO charge of the groups is defined as the sum over the NBO charge of each atom that constitutes the group under

Table 3
Some geometry parameters of the stationary points of the potential energy surface for R′=H and R′=CH_3[a]

Structure[b]	R′	C_2–C_{13}	C_3–C_{13}	C_2–C_{17}	C_3–C_{17}	C_2–C_{22}	C_{13}–C_{32}	C_{13}–C_{14}	C_{14}–C_{15}	C_{15}–C_{16}	C_{16}–C_{17}	C_{17}–C_{12}
3	H	3.352	3.688	—[c]	—[c]	—[c]	1.079	1.388	1.392	1.386	1.392	1.389
4		1.622	2.666	—[c]	—[c]	—[c]	1.090	1.487	1.358	1.398	1.423	1.352
6		3.857	—[c]	—[c]	—[c]	1.090	1.078	1.386	1.390	1.389	1.387	1.393
7		2.620	1.610	—[c]	—[c]	1.090	1.094	1.486	1.358	1.399	1.423	1.348
TS1		2.181	2.934	—[c]	—[c]	—[c]	1.078	1.414	1.382	1.384	1.408	1.370
TS2		—[c]	—[c]	—[c]	—[c]	1.325	1.078	1.386	1.389	1.388	1.386	1.393
TS3		2.910	2.195	—[c]	—[c]	1.093	1.076	1.410	1.388	1.381	1.413	1.364
3	CH_3	3.554	3.565	—[c]	3.761	—[c]	1.076	1.391	1.389	1.397	1.393	1.396
$\mathbf{4}_{ortho}$		3.513	—[c]	1.623	2.664	—[c]	1.074	1.435	1.379	1.381	1.498	1.502
$\mathbf{4}_{para}$		1.609	2.662	3.568	—[c]	—[c]	1.090	1.490	1.350	1.413	1.437	1.346
6		—[c]	—[c]	—[c]	—[c]	1.090	1.078	1.387	1.386	1.395	1.390	1.393
7		—[c]	—[c]	2.614	1.589	1.089	1.074	1.434	1.378	1.381	1.501	1.504
$\mathbf{7}_{para}$		2.617	1.604	—[c]	—[c]	1.090	1.093	1.489	1.350	1.414	1.438	1.343
$\mathbf{TS1}_{ortho}$		3.716	—[c]	2.322	3.019	—[c]	1.075	1.411	1.374	1.400	1.406	1.426
$\mathbf{TS1}_{para}$		2.342	3.032	3.745	—[c]	—[c]	1.078	1.405	1.382	1.391	1.414	1.371
TS2		—[c]	—[c]	—[c]	—[c]	1.332	1.078	1.387	1.386	1.395	1.390	1.393
$\mathbf{TS3}_{ortho}$		—[c]	3.657	3.004	2.277	1.093	1.075	1.414	1.372	1.402	1.414	1.492
$\mathbf{TS3}_{para}$		2.989	2.324	—[c]	3.718	1.094	1.076	1.404	1.387	1.388	1.419	1.365

[a] Bond distances are in Å and atom numbering according to Scheme 3.
[b] Structure numbering according to Scheme 1.
[c] Bond distance greater than 4.0 Å.

Table 4
The NBO charges of the groups[a] $E^{\oplus}$, Ar-R′, and H for the intermediate structures **3**[b] and **6**[b] and the transition state **TS2**[b]

Group[a]	**3**		**TS2**		**6**	
	R′=H	R′=CH_3	R′=H	R′=CH_3	R′=H	R′=CH_3
$E^{\oplus}$	1.926	1.933	1.922	1.911	1.909	1.913
Ar-R′	−0.151	−0.187	−0.151	−0.150	−0.140	−0.150
H[c]	0.224	0.255	0.225	0.237	0.230	0.239

[a] The definitions of $E^{\oplus}$, Ar-R′, and H groups are given in Scheme 3. The substituent of the aryl group R′ is part of the Ar group as defined in Scheme 3, nevertheless to discuss its influence on the charge of the group it is specified explicitly.
[b] The structure numbering is that given in Scheme 1. For the intermediate **3** the group $E^{\oplus}$ is a secondary carbocation while for the intermediate **6** is a benzylic carbocation.
[c] The H group is the acid H in the corresponding Wheland intermediate. In the products this H forms $BH^{\oplus}$ species.

Table 5
The NBO charges of the groups[a] $E^{\oplus}$, Ar-R′, and H for the transition states **TS1**[b] and **TS3**[b]

Group[a]	**TS1**			**TS3**		
	R′=H	R′=CH_3 *ortho*[c]	R′=CH_3 *para*[c]	R′=H	R′=CH_3 *ortho*[c]	R′=CH_3 *para*[c]
$E^{\oplus}$	1.628	1.691	1.705	1.599	1.621	1.657
Ar-R′	0.102	0.042	0.037	0.119	0.118	0.070
H[d]	0.272	0.266	0.259	0.279	0.263	0.268

[a] The definitions of $E^{\oplus}$, Ar-R′, and H groups are given in Scheme 3. The substituent of the aryl group R′ is part of the Ar group as defined in Scheme 3, nevertheless to discuss its influence on the charge of the group it is specified explicitly.
[b] The structure numbering is that given in Scheme 1. For the **TS1** transition state the group $E^{\oplus}$ is a secondary carbocation while for **TS3** transition state is a benzylic carbocation.
[c] In the *ortho* approach the $E^{\oplus}$ links to aryl group, Ar, through the carbon atom C_{17} while in *para* approach it is done through the carbon atom C_{13}. Atom numbering is according to Scheme 3.
[d] The H group is the acid H in the corresponding Wheland intermediate. In the products this H forms $BH^{\oplus}$ species.

consideration. In the intermediate cationic isomers **3** and **6** and the transition state **TS2**, the Ar group possesses a negative charge, while the E group has a positive charge near value two. The H group also has a positive charge. The charge on the Ar group depends on the substituent R′. When R′=CH_3, the charge of the Ar group is more negative than when R′=H. This result shows the well-known fact that the methyl group is electron donating while the hydrogen atom is electron withdrawing. In all the cases, the H group is weakly positive. The E group is positive near two due to the positive charge on the carbocation atom and the protonated amino group. The amino group remains positive charged during all the reaction evolution. In Table 5 we report the charge of the groups, E, Ar, and H for the transition states, **TS1** and **TS3**, which transform the intermediates **3** and **6** to the respective Wheland complexes **4** and **7**, respectively (Scheme 1). In both transition states the positive charge of the E group is lower but in the Ar group it is greater with respect to the corresponding intermediates **3** and **6**. Also the positive charge has been increased in the H group. The meaning of this effect is that in the transition states that transform the intermediates to Wheland complex, already an important fraction of electron density has been transferred from the Ar and H groups to the E group. For the **TS3** transition state the increase of positive charge in both Ar and H groups is greater than in **TS1**, and for both transition states the increase of positive charge in the Ar group is greater for R′=H than for R′=CH_3. Finally, the group charges of the Wheland complexes **4** and **7** are reported in Table 6. In both structures the positive charge of the E group is near one, which is mainly due to the protonated amino group. The positive charge of the Ar group is slightly superior when R′=CH_3 than when R′=H, this tendency is the inverse to that found in the transition state structures, **TS1** and **TS3**. The H group possesses more positive charge in the Wheland complexes than in the corresponding transition states, which means that as the reaction evolves it increases its acid character. The Wheland complex **7** has greater acid character than the Wheland complex **4**.

Table 6
The NBO charges of the groups[a] $E^{\oplus}$, Ar-R′, and H for the Wheland complexes **4**[b] and **7**[b]

Group[a]	**4**			**7**		
	R′=H	R′=CH_3 *ortho*[c]	R′=CH_3 *para*[c]	R′=H	R′=CH_3 *ortho*[c]	R′=CH_3 *para*[c]
$E^{\oplus}$	1.186	1.169	1.161	1.146	1.103	1.129
Ar-R′	0.516	0.555	0.548	0.537	0.620	0.567
H[d]	0.299	0.277	0.291	0.317	0.277	0.307

[a] The definitions of $E^{\oplus}$, Ar-R′, and H groups are given in Scheme 3. The substituent of the aryl group R′ is part of the Ar group as defined in Scheme 3, nevertheless to discuss its influence on the charge of the group it is specified explicitly.
[b] The structure numbering is that given in Scheme 1. The Wheland complex **4** results from the addition to the aryl group, Ar, the group $E^{\oplus}$, which is a secondary carbocation, while the Wheland complex **7** results from the addition to aryl group a benzylic carbocation.
[c] In the *ortho* approach the $E^{\oplus}$ links to aryl group, Ar, through the carbon atom C_{17} while in *para* approach it is linked through the carbon atom C_{13}. In the main text the intermediates **4** and **7** for R′=CH_3 are also denoted by $\mathbf{4}_{ortho}$, $\mathbf{4}_{para}$, $\mathbf{7}_{ortho}$, and $\mathbf{7}_{para}$. Atom numbering is according to Scheme 3.
[d] The H group is the acid H in both Wheland complex intermediates. In the products this H forms $BH^{\oplus}$ species.

4. Analysis and discussion

4.1. The valence bond representation of the electronic distribution of transition structures and intermediates

According to the computational results so far exposed in the previous section, the reaction depicted in Scheme 1 takes place through intermediates and transition states. Now we focus our attention on the reactions that transform the intermediate **3** to the product **5** and the intermediate **6** to the product **8**. These two competitive cyclizations fall into the well-known mechanism labeled as electrophilic aromatic substitution.[43,44] In this mechanism, the aromatic ring acts as a nucleophile giving a pair of its π-electrons to an electrophilic species, in the present case a carbocation. The leading species is a σ-complex intermediate, called Wheland complex, which is a benzenium or cyclohexadienylium type cation. This intermediate can be seen as a protonated aromatic compound that in a subsequent step releases the proton to a base and the resulting product regains the aromatic character, completing the reaction. The last step is normally very fast from a kinetic point of view and due to this fact has not been treated in the present study. The electrophilic aromatic substitution reactions have been considered extensively from a theoretical point of view, see e.g., the recent research of Houk and co-workers,[46] but the pioneer studies on these types of reactions were reported by Bertran and co-workers.[47,48]

The basic topic of this section is the idea that the RPES may be generated and analyzed from a linear combination of appropriate VB electronic distributions, where each one represents a specific type of wave function, associated to a chemical structure. In addition and following the discussion of Section 1, we describe the TS points of the PES or RPES by the wave function that describes the corresponding avoided crossing points, Ψ_{ACS}, a point, which is near to the TS points. As pointed out before, the wave function Ψ_{ACS} is build in terms of effective VB configurations. We note that this procedure has been applied several times[26] forming the basis of the so-called TS paradigm.[22,27]

Now, we regard the VB configurations and we will need to define the form of the RPES of an electrophilic aromatic substitution, whose more general view can be written as

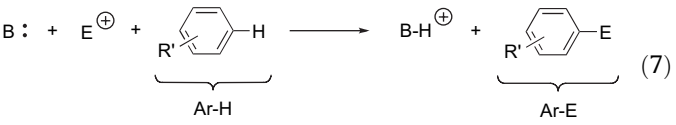

(7)

and the VB configurations that contribute are reported in Scheme 2. Let us consider each one of the VB configurations and their energies as a function of the two geometry parameters that describe the RPES (Fig. 1). The configuration Φ_{Reactant} is associated to the description of the electron distribution, which one finds in the reactants. The energy of this VB configuration, $E_{\Phi_{\text{Reactant}}}$, will move up as the reaction proceeds to the products. The reason of this increase is the C_{Ar}–H bond breaking, being C_{Ar} a carbon atom of the aromatic ring, and the formation on one hand, of a repulsive three electron interaction between B: and •H and on the other hand, the $C_{Ar}^{\bullet}E^{\oplus}$ bond formation a bond stabilized by an electron only.

With respect to the VB product configuration, Φ_{Product}, its energy value, $E_{\Phi_{\text{Product}}}$, is high in the reactant geometry configuration and lower in the product geometry configuration. The Φ_{Product} configuration describes an electron distribution resulting from the one electron excitation of Φ_{Reactant} electronic configuration. An electron of the base, B: has been transferred to the carbocation group $E^{\oplus}$. In this manner, the initial electron distribution in reactants B: $E^{\oplus}$ now is transformed as $B^{\bullet\oplus}$ •E a diradical cation and therefore unstable. This is the reason why $E_{\Phi_{\text{Reactant}}} < E_{\Phi_{\text{Product}}}$ is in the reactant geometry. At this point it is important to observe that in products exist stable interactions such that do not exist in the reactants, such as the B–H and C_{Ar}–E bonds, being C_{Ar} a carbon atom of the aromatic ring. Nevertheless, as the reaction evolves from reactants to products, the bond distances, d (E···Ar) and d (B···H···Ar–E), decrease and the stabilization become important, being this the reason why in the geometry of the products $E_{\Phi_{\text{Reactant}}} < E_{\Phi_{\text{Product}}}$.

There are many VB configurations for the reaction system 7 because many possibilities exist to distribute 10 electrons within eight centers. However, we look for configurations with sufficient low energy that play an important weight to generate or to construct the appropriate form of the RPES as depicted in Figure 1. According to the computational results exposed in the previous section, ionic intermediates are formed, so these are the most likely VB configurations. In Scheme 2 is illustrated a picture of the carbanionic VB configuration, $\Phi_{\text{Intermediate A}}$, which is related with a σ-type aryl carbanion and the carbocationic VB configuration, $\Phi_{\text{Intermediate C}}$, related with a Wheland complex. These two added VB configurations are different with respect to the reactant and product configurations and due to this fact they have different energy profiles.

The shape of the energy associated to the ionic VB configurations is a function of the type of the geometric parameters used to describe the evolution of these configurations from reactants to products. If we consider that the mechanistic situation described by the path where the bond breaking C_{Ar}–H and bond formation C_{Ar}–E occur in a synchronous manner, the energy associated to the ionic configurations, $E_{\Phi_{\text{Intermediate A}}}$ and $E_{\Phi_{\text{Intermediate C}}}$, is almost constant through this pathway. At the geometry of reactants $E_{\Phi_{\text{Intermediate A}}} > E_{\Phi_{\text{Reactant}}}$ because an electron has been moved from the base B: to a carbon atom of the aromatic ring, C_{Ar}:, resulting in a three electron structure, $C_{Ar}{:}^{\bullet}H^{\ominus}$, which is unstable and a $B^{\bullet\oplus}$. When the reaction evolves, the $C_{Ar}{:}^{\bullet}H^{\ominus}$ is breaking and forming the B–H bond. For this last, the initial instability of the form $C_{Ar}{:}^{\bullet}H^{\ominus}$ is released, and by approximation of $C_{Ar}{:}^{\ominus}$ to the carbocation $E^{\oplus}$ the C_{Ar}–E bond is made. These two effects drop slightly the energy of the carbanionic VB configuration $\Phi_{\text{Intermediate A}}$ as the reaction goes from reactants to products. However, the $E_{\Phi_{\text{Intermediate A}}}$ is very high at each point of the PES region related with the reaction under consideration, since it involves a σ-type aryl carbanion and for this reason will not be considered in the latter VB analysis. Finally, we considered the carbocationic configuration, $E_{\Phi_{\text{Intermediate C}}}$. At the reactant geometry an electron has been transferred from π-aromatic system, Ar–H, to the carbocation, $E^{\oplus}$, and due to this fact the aromatic character is lost being the reason that at this point of the PES $E_{\Phi_{\text{Intermediate C}}} > E_{\Phi_{\text{Product}}} > E_{\Phi_{\text{Reactant}}}$. Similar situation occurs at the product geometry, where an electron from the π-aromatic system, Ar–E, has been transferred to the B–H, leading to a three electron form B:H•, which is unstable. These two factors are the reason why $E_{\Phi_{\text{Intermediate C}}} > E_{\Phi_{\text{Reactant}}} > E_{\Phi_{\text{Product}}}$ at the product geometry. Nevertheless, at some points of the PES located between reactants and products $\Phi_{\text{Intermediate C}}$ diminishes its energy with respect to the energies of Φ_{Reactant} and Φ_{Product} due to the relative stabilization of E–Ar–$H^{\oplus}$. In Figure 3A is shown a graphic of these general qualitative results. On the other hand, in Figure 3B is shown the qualitative behavior of the bonding and antibonding wave functions whose mathematical forms are that given in Eqs. 5 and 6, respectively. They were built according to it was explained in VB description of Sections 1 and 2. In the avoided crossing points the bonding wave function possesses the mathematical form given in Eq. 1.

According to the above discussion, the normalized wave function describes the electronic state of the TS and can be expressed taking Eq. 2 with N=1 and the VB structures, which are now $\Phi_{\text{HL}}(\text{R}) \rightarrow \Phi_{\text{Reactant}}$, $\Phi_{\text{HL}}(\text{P}) \rightarrow \Phi_{\text{Product}}$, and $\Phi_I \rightarrow \Phi_{\text{Intermediate C}}$, for the case of the **TS1** and **TS3**. Following Shaik et al.,[27,49] the mixing coefficients, $c'_{\text{Reactant}}=c'_{\text{R}}$, $c'_{\text{Product}}=c'_{\text{P}}$ and $c'_{\text{Intermediate C}}=c'_{\text{IC}}$, are evaluated from the absolute magnitudes of the group charges given in Scheme 2, in accord to the set of equations,

$$|q(\text{E}^{\oplus})|^{1/2} = c'_{\text{R}};\quad |q(\text{Ar}^{\oplus})|^{1/2} = c'_{\text{IC}};\quad |q(\text{H}^{\oplus})|^{1/2} = c'_{\text{P}} \tag{8}$$

In Table 7 are shown the VB coefficients, c'_{R}, c'_{P} and c'_{IC}, for the **TS1** and **TS3** transition states and for R′=H and R′=CH_3. For the case R′=CH_3 are exposed the *ortho* and *para* approximations. An inspection of Table 7 reveals that the most important VB configurations are the Heitler–London configurations, which are the electronic distributions of reactants and products, as discussed in Section 2. In all cases, it is shown that $c'_{\text{R}} > c'_{\text{P}} > c'_{\text{IC}}$, which means that the TS wave function has an excess of reactant configuration. For both **TS1** and **TS3** transition states, the c'_{R} coefficient increases as R′=H is changed by the methyl radical, and when this group is located in *para* position then c'_{R} coefficient takes the largest value. The reverse situation is done for the coefficients c'_{P} and c'_{IC}, however, this variation is more important for the c'_{IC} coefficient, which is related with the Wheland complex. The c'_{R} coefficient is lower for the **TS3** than that for the **TS1** case. We also conclude that the weight of the Wheland complex electronic distribution decreases when increasing the electron-donating character of the R′ group linked to the aromatic ring.

The information reported from the TS wave function analysis gives support to the well-known facts that for electron-donating substituents (R′) like methyl radical, linked to the aryl group, the position of the TS is *earlier* with respect to the reactants and *later* if the $E^{\oplus}$ group is the benzilic carbocation, which is more stable than a secondary carbocation like **3**. Since in any case $c'_{\text{R}} \neq c'_{\text{P}}$ we conclude that the **TS1** and **TS3** are not located in the crossing point of reactant and product VB configurations. The **TS1** and **TS3** geometries should be located in a position of the reaction path where $E_{\Phi_{\text{Reactant}}} < E_{\Phi_{\text{Product}}} < E_{\Phi_{\text{Intermediate C}}}$ because $c'_{\text{R}} > c'_{\text{P}} > c'_{\text{IC}}$. The asymmetry in both transition states of the avoided crossing between reactants and products is due to the E–Ar–$H^{\oplus}$ contribution to the Heitler–London VB electronic distributions. This means that at large distance between $E^{\oplus}$ and Ar–H in the region located on the left-hand side of the avoided crossing point the mixing of E–Ar–$H^{\oplus}$ will be smaller than on the right-hand side of this crossing point where the

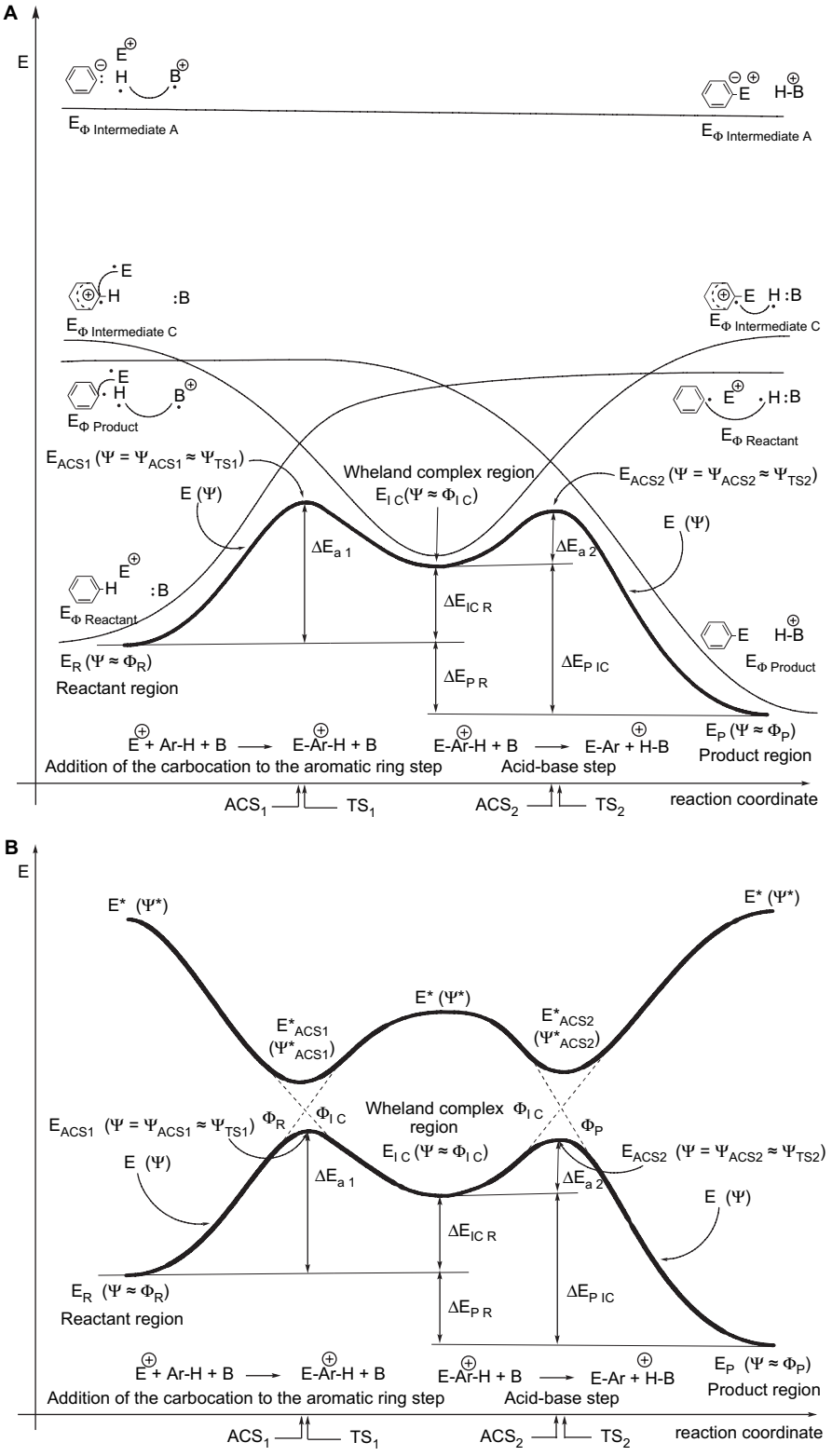

Figure 3. (A) A generic VBCM diagram for an electrophilic aromatic substitution reaction. The thin curves denote the energy profiles of the VB states, $E_{\Phi I}$, while the bold curve denotes the potential energy profile of the ground bonding electronic state, $E(\Psi)$, and the subscript ΦI, denotes the VB configuration, I=reactant, product, intermediate C, intermediate A, as defined in Scheme 2. The points in the E curve, ACSx and TSx, being x=1 or 2, are the avoided crossing structure and its near transition state structure, respectively. The ΔE_{ax} and ΔE_{KL} are the barriers and reaction energies, respectively, being K=IC or P and L=R or IC. The meaning of E, Ar, H, and B are given in Scheme 2. Notice that at the ACSx points $\Psi = \Psi_{ACS_x} - \Psi_{TS_x}$, as given in Eq. 1 or Eqs. 9 and 11. The energy profile, $E(\Psi)$, corresponds to the mechanism involving the intermediate C of Figure 1. (B) A generic generation of the bonding electronic state, $E(\Psi)$, and the corresponding antibonding state, $E^*(\Psi^*)$, for the electrophilic aromatic substitution. Both the Ψ and Ψ^* wave functions are build from the VB configurations described in (A) and Scheme 2. The mathematical expression of these two wave functions is given in Eqs. 5 and 6. The potential energy profiles generated by these electronic states along the reaction coordinate are depicted in bold curves. The meaning of the symbols are the same of Figure 3A. In the avoided crossing points we have for the antibonding state, $\Psi^* = \Psi^*_{ACS_1} = 2^{-1/2}[\Phi_R - \Phi_{IC}]$ and $\Psi^* = \Psi^*_{ACS_2} = 2^{-1/2}[\Phi_{IC} - \Phi_P]$, while in the Wheland complex region $\Psi^*=2^{-1/2}[\Phi_R-\Phi_P]$. The energy profile of $E(\Psi)$ corresponds to the mechanism involving the intermediate C of Figure 1.

Table 7
Coefficients of VB configurations for the transition states **TS1** and **TS3** evaluated according to Eq. 8 [a]

Coefficient	**TS1**			**TS3**		
	R′=H	R′=CH_3 *ortho*	R′=CH_3 *para*	R′=H	R′=CH_3 *ortho*	R′=CH_3 *para*
c'_R	0.792	0.831	0.840	0.774	0.788	0.811
c'_P	0.522	0.506	0.509	0.528	0.513	0.518
c'_{IC}	0.319	0.205	0.192	0.345	0.344	0.265

[a] **TS1** is the transition state generated by the addition of the secondary carbocation $E^{\oplus}$ to the aryl group Ar-R′. The same for the **TS3** transition state except that $E^{\oplus}$ group is a benzyl carbocation. The definitions of the groups $E^{\oplus}$ and Ar-R′ are given in Scheme 3. The R′ is part of the Ar group. The structure numbering is that given in Scheme 1. In the main text, for R′=CH_3, the corresponding isomer structures of **TS1** and **TS3** are denoted by **TS1**$_{ortho}$, **TS1**$_{para}$, **TS3**$_{ortho}$, and **TS3**$_{para}$.

distance between $E^{\oplus}$ and Ar–H is shorter than given rise to the Wheland complex intermediate. In other words, we conclude that for these series of electrophilic aromatic substitutions, the geometries of first TS and the avoided crossing point do not coincide, so they are only somewhat apart. This conclusion has some parallelism with that reported by Shaik et al. in their studies on the ionic S_N2 reactions.[49] However, we assume that in the present the electrophilic aromatic substitution reactions, the first TS and the avoided crossing point are closer points in the PES and the effects of E–Ar–$H^{\oplus}$ contribute to shift one point with respect to the other. This shift between the TS and the avoided crossing point was proved rather than assumed for the ionic S_N2 reactions.[49]

Taking into account the geometric features **TS1** and **TS3** for R′=H, CH_3 *ortho*, and CH_3 *para*, bond distance *d* (E···Ar) has the smallest value for R′=H, and the largest for R′=CH_3 *para*. Based on the values reported in Table 7, the VB coefficients c'_R for each TS type increase in the same direction. In addition, the bond distance *d* (E···Ar) is smaller for **TS3** than for **TS1**, except for R′=H that is almost equal. The VB coefficients c'_R are smaller for **TS3** than for **TS1**. The bond distance *d* (B···H···Ar) remains constant for all situations and it is equal to the standard bond distance *d* (H···C_{Ar}) being C_{Ar} the carbon atom of the aryl group where at the products is linked with E. Clearly, we can conclude that the formation of Wheland complexes follows the Bell–Evans–Polanyi (BEP)[50] and related principles,[15–21] and the VB analysis of the TS goes in the same direction.

We translate the above results to the RPES model. As briefly described in Section 1, the RPES model predicts the new position of the TS due to modification of the reactants. According to the previous explanations, the formation of the Wheland complexes can be explained using both the BEP and the VBCM models. The BEP principle, the VBCM, and the RPES models are strongly related. For all these models the TS structure is built and analyzed as a hybrid of some VB structures. The main difference between these models resides in the relation between the TS and the VB structures. Whereas the BEP and VBCM models assume that the TS structure is located near the crossing point of the Heitler–London VB structures of reactants and products and weakly affected by other VB structures, in the RPES model four VB structures are considered related with reactants, products, and two intermediates, and the degree of mixing in the TS structure depends of the charge of each basic structure. Thus BEP principle can be formulated in terms of VBCM model because for this principle the TS is located in a region, which is very near to the seam of the avoided crossing of the reactant and product configurations, in other words, $\Psi_{TS} \approx \Psi_{ACS} \approx 2^{-1/2}[\Phi_{HL}(R)+\Phi_{HL}(P)]$, where the intermediate configurations that appear in Ψ_{ACS} are not taken into account or assumed to be small, $c_I \approx 0$, for $I=1, N$.[27,33,49,51] However, the RPES model is more appropriated to describe stepwise reactions as in the present case but the main difference with respect to the BEP and VBCM models is in the way to mix the selected basis of VB structures. If in the RPES model, the rule of mixing the basic four VB structures is changed for that given in Eq. 5, then this model can be formulated in terms of the VBCM model. In other words, the RPES can be built through the VBCM wave function. Figure 1 helps to establish a general view of the relation between RPES and VBCM models, since in this RPES exist five avoided crossing points, which are near to the corresponding five transition states. In these avoided crossing points the wave function takes the mathematical form given in Scheme 5. Nevertheless, in the present case the $\Phi_{\text{Intermediate A}}$ VB configuration does not have any weight for the reasons explained above.

Two step mechanism through the intermediate A:

$$\begin{cases} \Psi_{TS\,A1} - \Psi_{ACS\,A1} = (1 + c^2_{I\,C} + c^2_P)^{-1/2}\{2^{-1/2}[\Phi_R + \Phi_{I\,A}] + c_{I\,C}\,\Phi_{I\,C} + c_P\,\Phi_P\} \\ \Psi_{TS\,A2} - \Psi_{ACS\,A2} = (1 + c^2_{I\,C} + c^2_R)^{-1/2}\{2^{-1/2}[\Phi_{I\,A} + \Phi_P] + c_{I\,C}\,\Phi_{I\,C} + c_R\,\Phi_R\} \end{cases}$$

Two step mechanism through the intermediate C:

$$\begin{cases} \Psi_{TS\,C1} - \Psi_{ACS\,C1} = (1 + c^2_{I\,A} + c^2_P)^{-1/2}\{2^{-1/2}[\Phi_R + \Phi_{I\,C}] + c_{I\,A}\,\Phi_{I\,A} + c_P\,\Phi_P\} \\ \Psi_{TS\,C2} - \Psi_{ACS\,C2} = (1 + c^2_{I\,A} + c^2_R)^{-1/2}\{2^{-1/2}[\Phi_{I\,C} + \Phi_P] + c_{I\,A}\,\Phi_{I\,A} + c_R\,\Phi_R\} \end{cases}$$

Single step mechanism:

$$\Psi_{TS\,S} - \Psi_{ACSS} = (1 + c^2_{I\,A} + c^2_{I\,C})^{-1/2}\{2^{-1/2}[\Phi_R + \Phi_P] + c_{I\,A}\,\Phi_{I\,A} + c_{I\,C}\,\Phi_{I\,C}\}$$

Scheme 5.

Using this new approach between RPES and VBCM models, we can propose conditions for the possible Friedel–Crafts mechanisms be single step or stepwise. Regarding Figure 3A we can derive this set of conditions. In the reactant region, small gap between the energy curves is associated to the VB structures Φ_{Reactant} and $\Phi_{\text{Intermediate C}}$ and large separation between the energy curves is associated to Φ_{Reactant} and Φ_{Product}. This last leads to a stepwise mechanism that involves first an addition to the aromatic ring and second acid–base phases. Such situation arises if the aryl substituents are electron-withdrawing and the base is weak. On the other hand, if the aryl substituents are electron-donating and the Brønsted base is strong, which implies that in the region of reactants the energy curves associated to Φ_{Reactant} and Φ_{Product} are close, see Figure 3A, a single-step mechanism will take place. The latter situation corresponds to the diagonal path in the More O'Ferrall–Albery–Jencks diagram (Fig. 1), while the former corresponds to the pathway composed by the left-vertical line followed by the horizontal line. We conclude saying that for the Friedel–Crafts rearrangement the RPES model can be formulated also in terms of VBCM model and both can be used to decide the structure of the mechanism.

To explore the possibility that the present reaction takes place through a single step rather than stepwise, and having assumed the proximity of the TS to the avoided crossing point, regarding Figure 3, the following Ψ_{ACS} wave function was built

$$\Psi_{ACS_1} = \left(1 + c_P^2\right)^{-1/2}\left\{2^{-1/2}[\Phi_{HL}(R) + \Phi_{\text{Intermediate C}}] + c_P\Phi_{HL}(P)\right\} \quad (9)$$

In the Ψ_{ACS_1} wave function the two Heitler–London configurations describe the structures of reactants and the intermediate or Wheland complex in others words the resonating state is defined by the VB configurations $\Phi_{HL}(R)$ and $\Phi_{\text{Intermediate C}}$. The Ψ_{ACS_1} wave function takes the mathematical form given in Eq. 9 in the avoided crossing point located in the region of the PES that lies directly beneath the crossing point of $\Phi_{HL}(R)$ and $\Phi_{\text{Intermediate C}}$. Regarding Figure 3A, the avoided crossing point, ACS_1, is the point of the PES where the Ψ_{ACS} wave function takes the form of that given in

Eq. 9 and the **TS1** is likely to lie very close to one another concluding that the reaction takes place in a stepwise mechanism. Therefore one concludes that $\Psi_{TS_1} \approx \Psi_{ACS_1} \approx \Psi$. The charge distribution of the $\Psi_{TS_1} \approx \Psi_{ACS_1}$ follows Eq. 10,

$$|q(E^{\oplus})|^{1/2} = |q(Ar^{\oplus})|^{1/2} = \frac{1}{2(1+c_P^2)}; \quad |q(H^{\oplus})|^{1/2} = \frac{c_P^2}{1+c_P^2} \tag{10}$$

On the other hand looking again Figures 1 and 3, for the single-step mechanism the wave function at the avoided crossing point is,

$$\Psi_{ACS_S} = \left(1+c_{IC}^2\right)^{-1/2}\left\{2^{-1/2}[\Phi_{HL}(R)+\Phi_{HL}(P)] + c_{IC}\Phi_{\text{Intermediate C}}\right\} \tag{11}$$

where the resonating Heitler–London state is described by the two VB configurations $\Phi_{HL}(R)$ and $\Phi_{HL}(P)$. As mentioned many times, here $\Psi_{ACS_S} \approx \Psi_{TS_S}$, where TS_S is the transition state of the single-step mechanism. The charge distribution of the $\Psi_{TS_S} \approx \Psi_{ACS_S}$ follows Eq. 12,

$$|q(E^{\oplus})|^{1/2} = |q(H^{\oplus})|^{1/2} = \frac{1}{2(1+c_{IC}^2)}; \quad |q(Ar^{\oplus})|^{1/2} = \frac{c_{IC}^2}{1+c_{IC}^2} \tag{12}$$

To find the Ψ_{ACS_1} and Ψ_{ACS_S} wave functions with the best fit to the Ψ_{TS1} and Ψ_{TS_S} wave functions, respectively, we proceed to minimize the 'distance' function between the both wave functions, defined as[49]

$$\Delta = \|\Psi_{TSx} - \Psi_{ACSx}\|^2 = \left\{c'_R - \frac{1}{[2(1+c_I^2)]^{1/2}}\right\}^2 + \left\{c'_P - \frac{1}{[2(1+c_I^2)]^{1/2}}\right\}^2 + \left\{c'_{IC} - \frac{c_I}{[1+c_I^2]^{1/2}}\right\}^2 \tag{13}$$

where x=1 or S, c'_R, c'_P and c'_{IC} are the coefficients of the Ψ_{TS} given in Eq. 2 and c_I=c_P if we fit Ψ_{ACS_1} and c_I=c_{IC} if we fit Ψ_{ACS_S}. In Table 8 is shown the charge distribution of the Ψ_{TS} and the best fit Ψ_{ACS_1} and Ψ_{ACS_S} for **TS1** and **TS3**. The TS charges are computed from the NBO UHF level of calculations. We also report for each case the value of the minimum 'distance', Δ, as given in Eq. 13 for each best fit. From Table 8 we conclude that for both cases, **TS1** and **TS3**, the fitted charge distribution of the Ψ_{ACS_S} is quite close to the TS one, labeled as NBO TS, being the largest deviation 0.055. The total charge is equal one since the charge on the protonated amino group, –NH2$^{\oplus}$–, was not considered due to the fact that remains constant and equal one during all the reaction process. From these results we conclude that the present Friedel–Crafts reaction occurs through a single-step mechanism either for R′=H and R′=CH_3.

Table 8
Comparison between the NBO charges[a] of the groups[b] $E^{\oplus}$, Ar-R′, and H for the transition states **TS1** and **TS3** and the charges of these groups obtained from the best fit ACS wave function[c]

Transition state	Group[b] charges			$(c_I)^2$ [f]	$\Delta\times10^{-2}$ [g]
	$E^{\oplus}$	Ar-R′	H[h]		
TS1, *R′=H*					
NBO TS	0.628	0.102	0.272		
ACS_S[d]	0.447	0.105	0.447	$0.12_{(I=IC)}$	3.676
ACS_1[e]	0.347	0.347	0.307	$0.44_{(I=P)}$	11.500
TS1 *R′=CH_3 ortho*					
NBO TS	0.691	0.042	0.266		
ACS_S[d]	0.478	0.045	0.478	$0.05_{(I=IC)}$	5.390
ACS_1[e]	0.338	0.338	0.323	$0.48_{(I=P)}$	20.800
TS1 *R′=CH_3 para*					
NBO TS	0.705	0.037	0.259		
ACS_S[d]	0.481	0.039	0.481	$0.04_{(I=IC)}$	5.551
ACS_1[e]	0.337	0.337	0.327	$0.49_{(I=P)}$	22.220
TS3 *R′=H*					
NBO TS	0.599	0.119	0.279		
ACS_S[d]	0.438	0.123	0.438	$0.14_{(I=IC)}$	3.050
ACS_1[e]	0.346	0.346	0.308	$0.44_{(I=P)}$	9.440
TS3 *R′=CH_3 ortho*					
NBO TS	0.621	0.118	0.263		
ACS_S[d]	0.439	0.123	0.439	$0.14_{(I=IC)}$	3.810
ACS_1[e]	0.354	0.354	0.291	$0.41_{(I=P)}$	10.100
TS3 *R′=CH_3 para*					
NBO TS	0.657	0.070	0.268		
ACS_S[d]	0.463	0.074	0.463	$0.08_{(I=IC)}$	4.348
ACS_1[e]	0.342	0.342	0.317	$0.46_{(I=P)}$	15.540

[a] The NBO TS charges are computed from the UHF/6-311++G(d,p) level of theory. The charge of $-NH_2^{\oplus}-$ group is not taken into account, the total charge is equal one.
[b] The definitions of $E^{\oplus}$, Ar-R′, and H groups are given in Scheme 3. The R′ is part of the Ar group. For the **TS1** transition state the group $E^{\oplus}$ is a secondary carbocation while for **TS3** transition state it is a benzylic carbocation.
[c] The structure of the wave function at the ACS point is given in Eq. 1 taking N=1.
[d] ACS_S is the avoided crossing point near to the TS_S of the single-step mechanism of Figure 1. The wave function at this point is given in Eq. 11.
[e] ACS_1 is the avoided crossing point near to the TS_{C1} of the two-step mechanism of Figure 1, see also Figure 3. The wave function at this point is given in Eq. 9.
[f] The charges at the ACS_S and ACS_1 points are computed using Eqs. 12 and 10, respectively. Both equations are solely function of the coefficient c_1, being c_1=c_P for ACS_1 and c_1=c_{IC} for ACS_S.
[g] Either in ACS_1 or ACS_S situations, the used Ψ_{ACS} corresponds to the best fit with respect to the Ψ_{TS}, being Δ the values of the residual of the fit. The fit expression is given in Eq. 13.
[h] The H group is the acid H in the corresponding Wheland intermediate. In the products this H forms $BH^{\oplus}$ species. The structure numbering is that given in Scheme 1.

5. Conclusion

In this work the reaction mechanism of the *ortho*-allyl-*N*-benzylaniline transformation to dihydrodibenz[*b*,*e*]azepines and tetrahydrodibenz[*b*,*f*]azocines was explained from a computational quantum chemistry point of view. The main goal was to prove that the reaction occurs through a mechanism that falls into a Friedel–Crafts mechanistic scheme. Due to the structure of the mechanism it is proposed that the reaction behaves from a kinetic view as an intermediate case between an anti-Curtin–Hammett/Winstein–Holness and Curtin–Hammett/Winstein–Holness or anti-Curtin–Hammett/Winstein–Holness, if the aryl substituents are electron donating. We have used the VBCM model to build the avoided crossing state, Ψ_{ACS}, which provides a methodology for piecing up a reduced potential energy surface (RPES) and their reaction profiles from its component building blocks that are the selected basis of VB structures. Using the avoided crossing state as a paradigm to both construct and analyze the RPES, we report the conditions where a Friedel–Crafts reaction evolves through a single or stepwise mechanism. For the present Friedel–Crafts reaction the process occurs through a single-step mechanism. We conclude that VBCM model can be used as a way to analyze the BEP and RPES models, widely used in chemical reactivity studies.

Acknowledgements

The financial support from the projects, No. 1102-408-2056 (COLCIENCIAS), Spanish *Ministerio de Ciencia y Tecnología*, DGI project CTQ2005-01117/BQU and, in part from the *Generalitat de Catalunya* project 2005SGR-00111, are fully acknowledged. G. Tafurt-García gives thanks to *COLCIENCIAS* (*Instituto Colombiano para el Desarrollo de la Ciencia y la Tecnología*) by her scholarship of *Programa de Apoyo a Doctorados Nacionales-2003*. Finally we are grateful to A. Aguilar-Mogas and C. Rozo for helpful discussions.

References and notes

1. Briel, D. *Pharmazie* **1990**, *45*, 895.
2. Roeder, T.; Degen, J.; Gewecke, M. *Eur. J. Pharmacol.* **1998**, *349*, 171.
3. Sipido, V. K.; Fernández-Gadea, F. J.; Andrés-Gil, J. I.; Meert, T. F.; Gil-Lopetegui, P. PCT Int. Appl. WO 9614320, 1996; *Chem. Abstr.* **1996**, *125*, 142705g.
4. Andrés, J. I.; Alcázar, J.; Alonso, J. M.; Díaz, A.; Fernández, J.; Gil, P.; Iturrino, L.; Matesanz, E.; Meert, T. F.; Megens, A.; Sipido, V. K. *Bioorg. Med. Chem. Lett.* **2002**, *12*, 243.
5. Andersen, K. E.; Olsen, U. B.; Andersen, H. S.; Hohlweg, R.; Joergensen, T. K.; Madsen, P. PCT Int. Appl. WO 9631482, 1996; *Chem. Abstr.* **1997**, *126*, 8148v.
6. Joergensen, T. K.; Andersen, K. E.; Andersen, H. S.; Hohlweg, R.; Madsen, P.; Olsen, U. B. PCT Int. Appl. WO 9631497, 1996; *Chem. Abstr.* **1997**, *126*, 8146t.
7. Brugnara, C.; Halperin, J.; Bellott, E. M., Jr.; Froimowitz, M.; Lombardy, R. J.; Clifford, J. J.; Gao, Y.-D.; Haidar, R. M.; Kelleher, E. W.; Kher, F. M.; Moussa, A. M.; Sachdeva, Y.; Sun, M.; Taft, H. N.; Lencer, W. I.; Alper, S. PCT Int. Appl. WO 9926628, 1999; *Chem. Abstr.* **1999**, *131*, 18936t.
8. Fukumi, H.; Sakamoto, T.; Sugiyama, M.; Iizuka, Y.; Yamaguchi, T. U.S. Patent 5,476,848, 1995; *Chem. Abstr.* **1996**, *124*, 261063k.
9. Sinha, A. K.; Nizamuddin, S. *Ind. J. Chem.* **1984**, *23B*, 83.
10. (a) Sasakura, K.; Sugasawa, T. *Heterocycles* **1981**, *15*, 421; (b) Lypacewicz, M. K.; Poslinska-bucewka, H.; Smolinska, J.; Wasiak, T.; Sosinska, D.; Mostrak, M.; Trzpil, B.; Paszkowski, S. Pol. PL 175287, 1998; *Chem. Abstr.* **1999**, *130*, 296698x; (c) Stappers, F.; Broeckx, R.; Leurs, S.; Van den Bergh, L.; Agten, J.; Lambrechts, A.; Van den Heurel, D.; De Smaele, D. *Org. Process Res. Dev.* **2002**, *6*, 911.
11. Palma, A.; Barajas, J.; Kouznetsov, V.; Stashenko, E.; Bahsas, A.; Amaro-Luis, J. *Lett. Org. Chem.* **2004**, *1*, 261.
12. Palma, A.; Barajas, J.; Kouznetsov, V.; Stashenko, E.; Bahsas, A.; Amaro-Luis, J. *Synlett* **2004**, 2721.
13. Voskressensky, L. G.; Borisova, T. N.; Listratova, N. V.; Kulikova, L. N.; Titov, A. A.; Varlamov, A. V. *Tetrahedron Lett.* **2006**, *47*, 4585.
14. Arnold, L. A.; Guy, R. K. *Bioorg. Med. Chem. Lett.* **2006**, *16*, 5360.
15. Thornton, E. R. *J. Am. Chem. Soc.* **1967**, *89*, 2915.
16. More O'Ferrall, R. A. *J. Chem. Soc. B* **1970**, 274.
17. Harris, J. C.; Kurz, J. L. *J. Am. Chem. Soc.* **1970**, *92*, 349.
18. Albery, W. J. *Prog. React. Kinet.* **1967**, *4*, 355.
19. Jencks, W. P. *Chem. Rev.* **1972**, *72*, 705.
20. Grunwald, E. *J. Am. Chem. Soc.* **1985**, *107*, 125.
21. Bernasconi, C. F. *Acc. Chem. Res.* **1987**, *20*, 301.
22. Shaik, S. S.; Schlegel, H. B.; Wolfe, S. *Theoretical Aspects of Physical Organic Chemistry: The S_N2 Mechanism*; John Wiley & Sons: New York, NY, 1992.
23. Anglada, J. M.; Besalú, E.; Bofill, J. M.; Crehuet, R. *J. Comput. Chem.* **2001**, *22*, 387.
24. Bofill, J. M.; Anglada, J. M. *Theor. Chem. Acc.* **2001**, *105*, 463.
25. Hirsch, M.; Quapp, W. *Theor. Chem. Acc.* **2005**, *113*, 58.
26. Pross, A.; Shaik, S. S. *Acc. Chem. Res.* **1983**, *16*, 363.
27. Shaik, S. S.; Reddy, A. C. *J. Chem. Soc., Faraday Trans.* **1994**, *90*, 1631.
28. Shaik, S.; Shurki, A. *Angew. Chem., Int. Ed.* **1999**, *38*, 586.
29. Evans, M. G.; Polanyi, M. *Trans. Faraday Soc.* **1938**, *34*, 11.
30. Warshel, A.; Weis, R. M. *J. Am. Chem. Soc.* **1980**, *102*, 6218.
31. Chang, Y.-T.; Miller, W. H. *J. Phys. Chem.* **1990**, *94*, 5884.
32. Minichino, C.; Voth, G. A. *J. Phys. Chem. B* **1997**, *101*, 4544.
33. Anglada, J. M.; Besalú, E.; Bofill, J. M.; Crehuet, R. *J. Comput. Chem.* **1999**, *20*, 1112.
34. Kim, Y.; Corchado, J. C.; Villà, J.; Xing, J.; Truhlar, D. G. *J. Chem. Phys.* **2000**, *112*, 2718.
35. Villà, J.; Bentzien, J.; Gonzalez-Lafont, A.; Lluch, J. M.; Bertran, J.; Warshel, A. *J. Comput. Chem.* **2000**, *21*, 607.
36. Schlegel, H. B.; Sonnenberg, J. L. *J. Chem. Theory Comput.* **2006**, *2*, 905.
37. Frisch, M. J.; Trucks, G. W.; Schlegel, H. B.; Scuseria, G. E.; Robb, M. A.; Cheeseman, J. R.; Montgomery, J. A., Jr.; Vreven, T.; Kudin, K. N.; Burant, J. C.; Millam, J. M.; Iyengar, S. S.; Tomasi, J.; Barone, V.; Mennucci, B.; Cossi, M.; Scalmani, G.; Rega, N.; Petersson, G. A.; Nakatsuji, H.; Hada, M.; Ehara, M.; Toyota, K.; Fukuda, R.; Hasegawa, J.; Ishida, M.; Nakajima, T.; Honda, Y.; Kitao, O.; Nakai, H.; Klene, M.; Li, X.; Knox, J. E.; Hratchian, H. P.; Cross, J. B.; Bakken, V.; Adamo, C.; Jaramillo, J.; Gomperts, R.; Stratmann, R. E.; Yazyev, O.; Austin, A. J.; Cammi, R.; Pomelli, C.; Ochterski, J. W.; Ayala, P. Y.; Morokuma, K.; Voth, G. A.; Salvador, P.; Dannenberg, J. J.; Zakrzewski, V. G.; Dapprich, S.; Daniels, A. D.; Strain, M. C.; Farkas, O.; Malick, D. K.; Rabuck, A. D.; Raghavachari, K.; Foresman, J. B.; Ortiz, J. V.; Cui, Q.; Baboul, A. G.; Clifford, S.; Cioslowski, J.; Stefanov, B. B.; Liu, G.; Liashenko, A.; Piskorz, P.; Komaromi, I.; Martin, R. L.; Fox, D. J.; Keith, T.; Al-Laham, M. A.; Peng, C. Y.; Nanayakkara, A.; Challacombe, M.; Gill, P. M. W.; Johnson, B.; Chen, W.; Wong, M. W.; Gonzalez, C.; Pople, J. A. *Gaussian 03, Revisión C01*; Gaussian: Wallingford, CT, 2004.
38. (a) Hariharan, P. C.; Pople, J. A. *Theor. Chim. Acta* **1973**, *28*, 213; (b) Francl, M. M.; Petro, W. J.; Hehre, W. J.; Binkley, J. S.; Gordon, M. S.; DeFrees, D. J.; Pople, J. A. *J. Chem. Phys.* **1982**, *77*, 3654; (c) Clark, T.; Chandrasekhar, J.; Schleyer, P. v. R. *J. Comput. Chem.* **1983**, *4*, 294.
39. Krishnan, R.; Binkley, J. S.; Seeger, R.; Pople, J. A. *J. Chem. Phys.* **1980**, *72*, 650.
40. Foster, J. P.; Weinhold, F. *J. Am. Chem. Soc.* **1980**, *102*, 7211.
41. Weinhold, F.; Landis, C. R. *Valency and Bonding: A Natural Bond Orbital Donor–Acceptor Perspective*; Cambridge University Press: Cambridge, UK, 2005.
42. Laidler, K. *Theory of Reaction Rates*; McGraw-Hill: New York, NY, 1969.
43. Isaacs, N. *Physical Organic Chemistry*; Longman Scientific & Technical: Essex, UK, 1995.
44. Anslyn, E. V.; Dougherty, A. *Modern Physical Organic Chemistry*; University Science Books: Sausalito, CA, 2006.
45. (a) Curtin, D. Y. *Rec. Chem. Prog.* **1954**, *15*, 111; (b) Eliel, E. L. *Experientia* **1953**, *9*, 91; (c) Winstein, S.; Holness, N. J. *J. Am. Chem. Soc.* **1955**, *77*, 5562; (d) Zefirov, N. S. *Tetrahedron* **1977**, *33*, 2719; (e) Seeman, J. I. *Chem. Rev.* **1983**, *83*, 83.
46. Gordillo, R.; Carter, J.; Houk, K. N. *Adv. Synth. Catal.* **2004**, *346*, 1175.
47. Branchadell, V.; Oliva, A.; Bertrán, J. *J. Mol. Catal.* **1988**, *44*, 285.
48. Branchadell, V.; Oliva, A.; Bertrán, J. *J. Chem. Soc., Perkin Trans. 2* **1989**, 1091.
49. Shaik, S.; Ioffe, A.; Reddy, A. C.; Pross, A. *J. Am. Chem. Soc.* **1994**, *116*, 262.
50. Dewar, M. J. S. *The Molecular Orbital Theory of Organic Chemistry*; McGraw-Hill Book Company: New York, NY, 1969.
51. Jensen, F. *J. Am. Chem. Soc.* **1992**, *114*, 1997.